HHS Public Access

Author manuscript

MRS Adv. Author manuscript; available in PMC 2020 May 13.

Published in final edited form as:

MRS Adv. 2020 ; 5(16): 815–823. doi:10.1557/adv.2020.47.

RNA Delivery via DNA-Inspired Janus Base Nanotubes for Extracellular Matrix Penetration

Ian Sands[1], **Jinhyung Lee**[1], **Wuxia Zhang**[1], **Yupeng Chen**[1]

[1]Department of Engineering, University of Connecticut, Storrs, CT.

Abstract

RNA delivery into deep tissues with dense extracellular matrix (ECM) has been challenging. For example, cartilage is a major barrier for RNA and drug delivery due to its avascular structure, low cell density and strong negative surface charge. Cartilage ECM is comprised of collagens, proteoglycans, and various other noncollagneous proteins with a spacing of 20nm. Conventional nanoparticles are usually spherical with a diameter larger than 50–60nm (after cargo loading). Therefore, they presented limited success for RNA delivery into cartilage. Here, we developed Janus base nanotubes (JBNTs, self-assembled nanotubes inspired from DNA base pairs) to assemble with small RNAs to form nano-rod delivery vehicles (termed as “Nanopieces”). Nanopieces have a diameter of ~20nm (smallest delivery vehicles after cargo loading) and a length of ~100nm. They present a novel breakthrough in ECM penetration due to the reduced size and adjustable characteristics to encourage ECM and intracellular penetration.

INTRODUCTION

Post-traumatic arthritis is a condition that effects 12% of the 5.8 million individuals suffering with osteoarthritis (OA) in the United States(1). After joints sustain such injuries, the stimulation of inflammatory mediators can cause degeneration of the chondrocyte extracellular matrix. Due to the avascular nature of cartilage tissue, the degradation of the chondrocyte extracellular matrix is irreversible and eventually leads to the development of osteoarthritis. Small defects in the cartilage can pose a serious challenge to maintain tissues and there are currently no clinically approved therapies to prevent acute post-traumatic arthritis.

It has been found from previous studies that RNA interference (RNAi) is a cellular systematic control that effects which genes are active and the degree to which they are expressed(2). The major challenge is delivering these RNA molecules into tissue as dense and compact as cartilage(3). Traditional nanoparticle drug carriers are spherical in shape and range from 50–60 nm in diameter (once loaded) which leads to limited success for RNA delivery into cartilage. Once assembled with RNA into nano-rod delivery vehicles, NPs have a diameter of ~20nm and a length of ~100nm as seen in Fig 1(4–6). This presents a novel breakthrough in ECM penetration due to their reduced size and adjustable characteristics to encourage ECM and intracellular penetration. Furthermore, the non-covalent bonding

Contacting author: Yupeng.chen@uconn.edu.

present between binding DNA base pairs is essential for its excellent biodegradability and low cytotoxicity profile(7–10).

JBNTs are comprised of self-assembled supramolecular structures which are further broken down into guanine and cytosine DNA base pairs. The hollow channels formed by these nanotubes are ideal for drug loading and the six-member rosette comprised of hydrogen bonding is essential for its low cytotoxicity profile. By controlled assembly between our nucleic acid cargos (in this case siRNA) with JBNT solution, long segmented Nanopieces are synthesized. They can be further separated via a regulated sonication process. Nanopiece formulations were assembled and their material properties were studied using DLS and Zeta potential measurements. Their morphological characteristics and distributions were analyzed by TEM (transmission electron microscopy) imaging. The RNA delivery abilities of Nanopieces with different formulations were determined in vitro using human chondrocytes. Nanopiece binding and ECM penetration was also studied in vitro using fluorescence and confocal microscopy. Results of this study provide in-depth characterizations of these Nanopieces along with evaluating their abilities of RNA delivery. Our data also determines how Nanopieces bind with and penetrate into cell ECM to understand their delivery mechanism.

EXPERIMENTS

Nanopiece Synthesis and Characterization

JBNTs module was synthesized using previously established procedures and NPs were further synthesized by mixing with varying doses of siRNA (AllStars Negative Control siRNA). Once assembled, each NP solution was subject to sonication using the (QSonica) at 100% amplitude for two and a half minutes. Zeta potential and DLS measurements were taken using Zetasizer Nano-Series (Malvern) and averaged to provide accurate ionic charge readings for each NP solution. TEM images were taken of each subsequent NP solution by negative staining with 3% uranyl acetate solution via mix method. Preliminary statistical analysis was conducted using ImageJ to characterize the average width and length of each NP formulation.

Culture Conditions and Transfection Analysis

NP solutions were cultured in combination with human chondrocytes (C28/I2 cells) stored at 37°C 5% CO_2. Cultured solutions included NP formulations with 15, 30, and 40μL JBNT each mixed with 2μL siRNA(AF-488). Fluorescence imaging using fluorescence imager (ZOE) took place at time points of 1, 2, 3, and 5 days to observe intracellular uptake of fluorescence signal over time. Confocal imaging using was used on NP formulations with 15, 30 and 40μL JBNT each mixed with 2μL siRNA(AF-488) to demonstrate the influence of ionic charge on intracellular transfection efficacy. DAPI and Rhodamine Phalloidin (Invitrogen) were used for nuclear and cytoskeletal staining respectively, and all confocal images were taken using a standard preset optical setting. Qualitative analysis was performed on each NP cultured sample to observe penetration efficacy and cellular uptake was observed through a 5 day confocal study.

RESULTS AND DISCUSSION

NP solutions containing standard non-fluorescent siRNA and fluorescence attached siRNA were measured separately for comparison and are provided below. (Table 1 and 2). The varying doses showed an increase in charge magnitude at smaller and larger ratio values. Due to high ionic repulsion, the size estimate of respective NPs decreased as charge magnitude increased. Standard siRNA loaded NPs showed a more dramatic increase in charge magnitude however nearly identical trends were followed for each table. From this data, candidates for cell transfection were chosen based on increase in positive ionic charge. 15 JBNT was chosen due to its nearly neutral charge and clotted morphology (Fig. 2) as a benchmark comparison to negative control cells. 30μL and 40μL would serve as increasingly promising candidates for intracellular penetration due to their positive charge, ideal dimensions, and natural negative charge of cartilage tissue.

Cell Transfection Candidates

With TEM images of each sample, preliminary statistical analysis was performed and ideal dimensions previously claimed were confirmed for transfection candidates. 10 images were taken from separate locations of each NP sample and 10 NPs were measured from each image to yield 50 NPs averaged per dose value. Average NP lengths ranged between 150 – 170 nm and width remained ~20nm for all NP solutions except the 40μL JBNT dose (Table 3 and Fig.). It is worth noting that due to the abnormal clotted morphology of neutrally charged 15 JBNT NPs, the average width was greater than the expected 20 nm range and the standard deviation increased as well. We expect this to be a result of the lack of ionic repulsion between NP segments that allow localized clotting to occur. All other samples showed clean and segmented NP morphology expected to dense ECM penetration.

Microscopy Studies

A multiple day study was performed using fluorescence microscopy to analyse time dependency of intracellular NP ingestion as seen in Figure 3. 40 JBNT was selected for this experiment due to its high ionic charge coupled with its ideal average width of 20nm. Day 1 to Day 5 trends include the reduction of fluorescence signal, but a clear indication that fluorescence signal is being internalized and absorbed from the surface of the cell. As the fluorescence migrates from the surface of the ECM to the intracellular matrix, signal intensity may reduce and become less localized. Due to this observation, confocal microscopy was used to perform qualitative analysis of GAG-to-NP interaction with respect to JBNT dose (Fig. 4) and time (Fig. 5). As expected, the 15 JBNT group provided results identical to the negative control cells cultured with drug loaded NPs. As dose and subsequent charge increased, cell transfection efficiency and efficacy increased and results demonstrated successful intracellular penetration.

NP delivery is seen to increase from Day 1 to Day 2, however a prominent signal intensity appears mostly on the surface of the cells where the GAG-NP interaction takes place. As time increases however, signal intensity decreases and intracellular ingestion progresses, indicating that due to the dense nature of cartilage, ECM penetration and migration is a time-dependent process that requires further study.

NPs present a high degree of customizability due to their potential for various surface modifications that can bolster multiple aspects of targeting behaviour in a variety of cell types(11–13). Surface PEGylation will be explored in order to establish a greater circulation time for systemic injections(14,15). Targeting ligands may also be attached to the surface of NP delivery vehicles to bypass immune response and target specific cell types. These NP solutions serve as much more than a single function drug delivery vehicle for local injection treatment. NPs also hold the potential to be incorporated into nanofiber scaffolds, used as surface coatings for implants, and outfitted to sustain efficient and effective systemic delivery throughout the body. The physiochemical versatility of these NPs serves as the conceptual foundation that will allow for further study regarding the treatment of multiple other diseases.

CONCLUSION

The purpose of this study was to establish a library of NPs characterized by DLS, zeta potential, and TEM for future applications regarding cell transfection. Through these methods of characterizations, we were able to select viable candidates with ideal dense ECM penetration parameters such as positive ionic charge, standard segmented morphology, and ~20nm width. This study confirms the effective penetration of ECM using these candidates with fluorescence tagged siRNA. This is a promising first step towards establishing an effective localized delivery method for difficult-to-reach tissues such as cartilage.

ACKNOWLEDGEMENTS

The authors would like to thank NIH (Grants 1R01AR072027-01, 1R03AR069383-01), NSF Career Award (1653702) and the Office of Undergraduate Research (OUR) at the University of Connecticut for providing funds to support this project.

REFERENCES:

[1]. Agrawal N, Dasaradhi PVN, Mohmmed A, Malhotra P, Bhatnagar RK, Mukherjee SK, RNA interference: biology, mechanism, and applications. Microbiol Mol Biol Rev 2003;67(4):657–85. [PubMed: 14665679]

[2]. Lotz MK, Kraus VB. New developments in osteoarthritis. Posttraumatic osteoarthritis pathogenesis and pharmacological treatment options. Arthritis Res Ther 2010;12(3):211. [PubMed: 20602810]

[3]. Trozilli PA, Arduino J,M, Gregory JD & Bansal M Effect of proteoglycan removal on solute mobility in articular cartilage. J. Biomech 1997; 30, 895–902. [PubMed: 9302612]

[4]. Chen Y, Song S, Yan Z, Fenniri H, Webster TJ. Self-assembled rosette nanotubes encapsulate and slowly release dexamethasone. Int J Nanomedicine 2011;6:1035–44. [PubMed: 21720515]

[5]. Moralez JG, Raez J, Yamazaki T, Motkuri RK, Kovalenko A, Fenniri H. Helical Rosette Nanotubes with Tunable Stability and Hierarchy. Journal of the American Chemical Society. 2005;127(23):8307–9. [PubMed: 15941263]

[6]. Song S, Chen Y, Yan Z, Fenniri H, Webster TJ. Self-assembled rosette nanotubes for incorporating hydrophobic drugs in physiological environments. International journal of nanomedicine. 2011;6:101–7. [PubMed: 21289987]

[7]. Zhang L, Chen Y, Rodriguez J, Fenniri H, Webster TJ. Biomimetic helical rosette nanotubes and nanocrystalline hydroxyapatite coatings on titanium for improving orthopedic implants. International journal of nanomedicine. 2008;3(3):323–33. [PubMed: 18990941]

[8]. Chen Y, Bilgen B, Pareta RA, Myles AJ, Fenniri H, Ciombor DM, et al. Self-Assembled Rosette Nanotube/Hydrogel Composites for Cartilage Tissue Engineering. Tissue Engineering Part C: Methods. 2010;16(6):1233–43. [PubMed: 20184414]

[9]. Journeay WS, Suri SS, Moralez JG, Fenniri H, Singh B. Rosette nanotubes show low acute pulmonary toxicity in vivo. International journal of nanomedicine. 2008;3(3):373–83. [PubMed: 18990946]

[10]. Zhang L, Rakotondradany F, Myles AJ, Fenniri H, Webster TJ. Arginine-glycine-aspartic acid modified rosette nanotube–hydrogel composites for bone tissue engineering. Biomaterials. 2009;30(7):1309–20. [PubMed: 19073342]

[11]. Zhang F, Lin Y-A, Kannan S, Kannan RM. Targeting specific cells in the brain with nanomedicines for CNS therapies. Journal of Controlled Release. 2016;240:212–26. [PubMed: 26686078]

[12]. Chu DSH, Schellinger JG, Bocek MJ, Johnson RN, Pun SH. Optimization of Tet1 ligand density in HPMA-co-oligolysine copolymers for targeted neuronal gene delivery. Biomaterials. 2013;34(37):9632–7. [PubMed: 24041424]

[13]. da Fonseca AC, Badie B. Microglia and macrophages in malignant gliomas: recent discoveries and implications for promising therapies. Clin Dev Immunol 2013;2013:264124. [PubMed: 23864876]

[14]. Suk JS, Xu Q, Kim N, Hanes J, Ensign LM. PEGylation as a strategy for improving nanoparticle-based drug and gene delivery. Adv Drug Deliv Rev 2016;99(Pt A):28–51 [PubMed: 26456916]

[15]. Abuchowski A, McCoy JR, Palczuk NC, van Es T, Davis FF. Effect of covalent attachment of polyethylene glycol on immunogenicity and circulating life of bovine liver catalase. J Biol Chem 1977;252(11):3582–6. [PubMed: 16907]

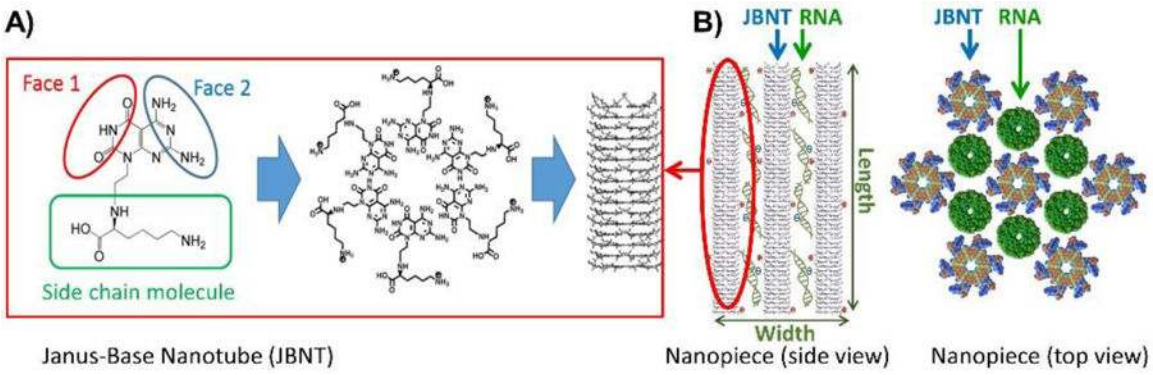

Figure 1.

Structure and assembly of A) JBNTs and B) NPs (NOTE: more layers of RNA and JBNT may be assembled in one NP, which determines its width).

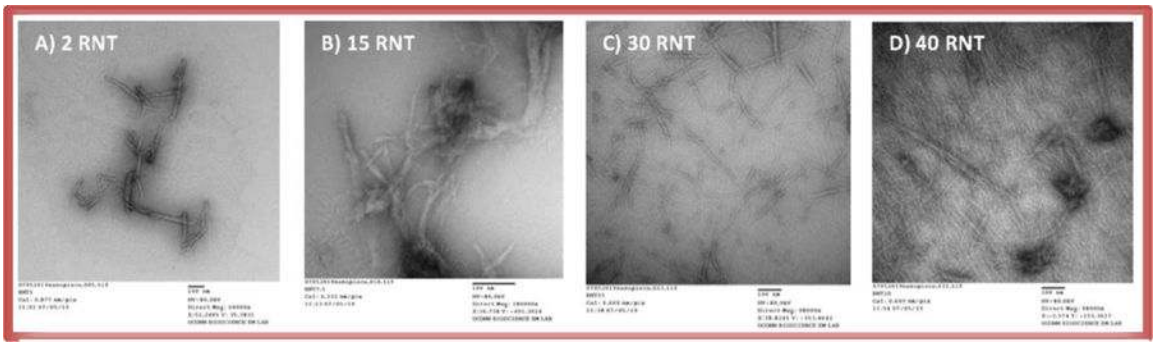

Figure 2.
TEM Images Taken of **A)** 2μL JBNT **B**) 15μL JBNT **C)** 30μL JBNT **D)** 40μL JBNT doses.

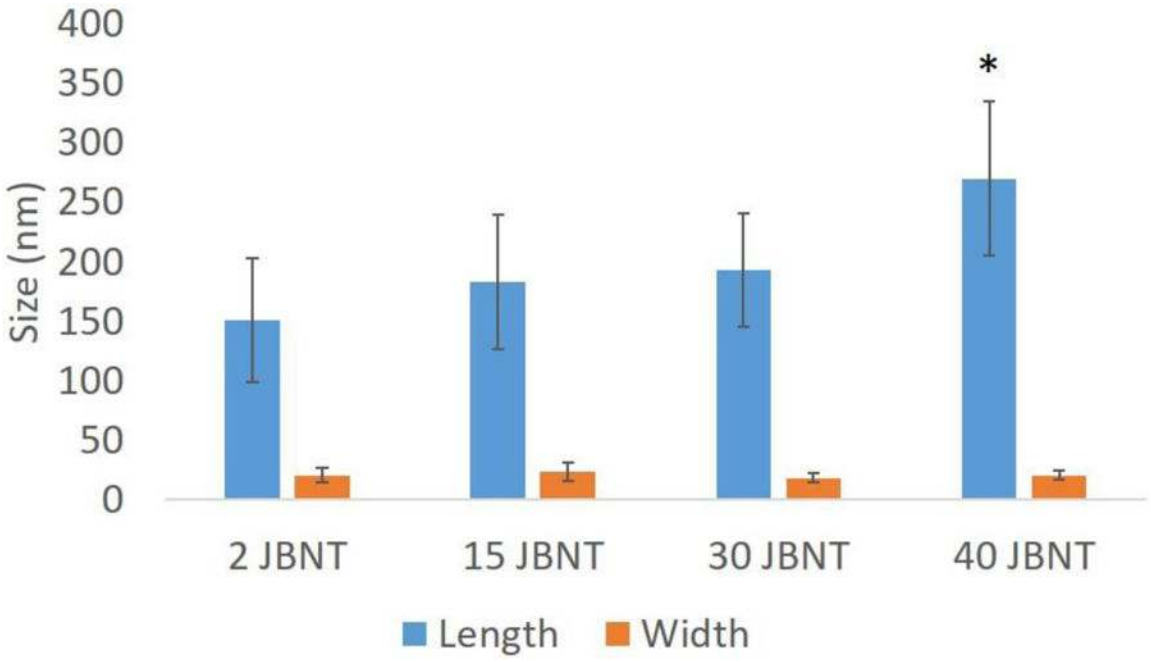

Figure 3.
Tabulated organization of JBNT doses ranging from 2–40μL with corresponding lengths and widths (at a 2μL siRNA dose). N=50. *p<0.05 compared with other groups.

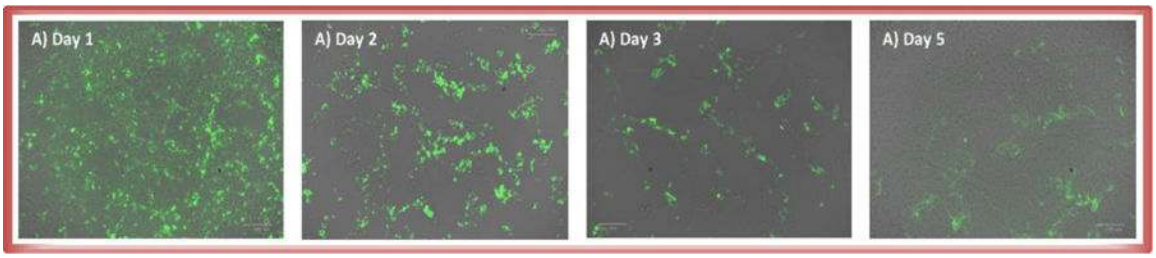

Figure 4.
Fluorescence signal internalization of NPs showing Day 1, 2, 3, and 5.

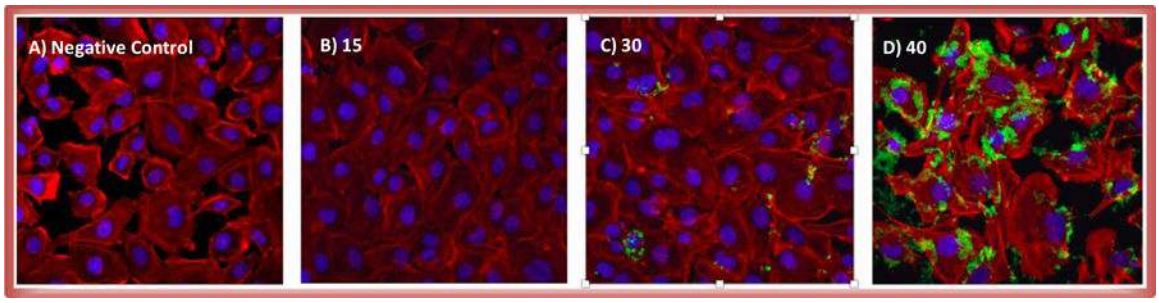

Figure 5.
Confocal microscopy results demonstrating increasing intracellular penetration efficacy of positively charged NPs

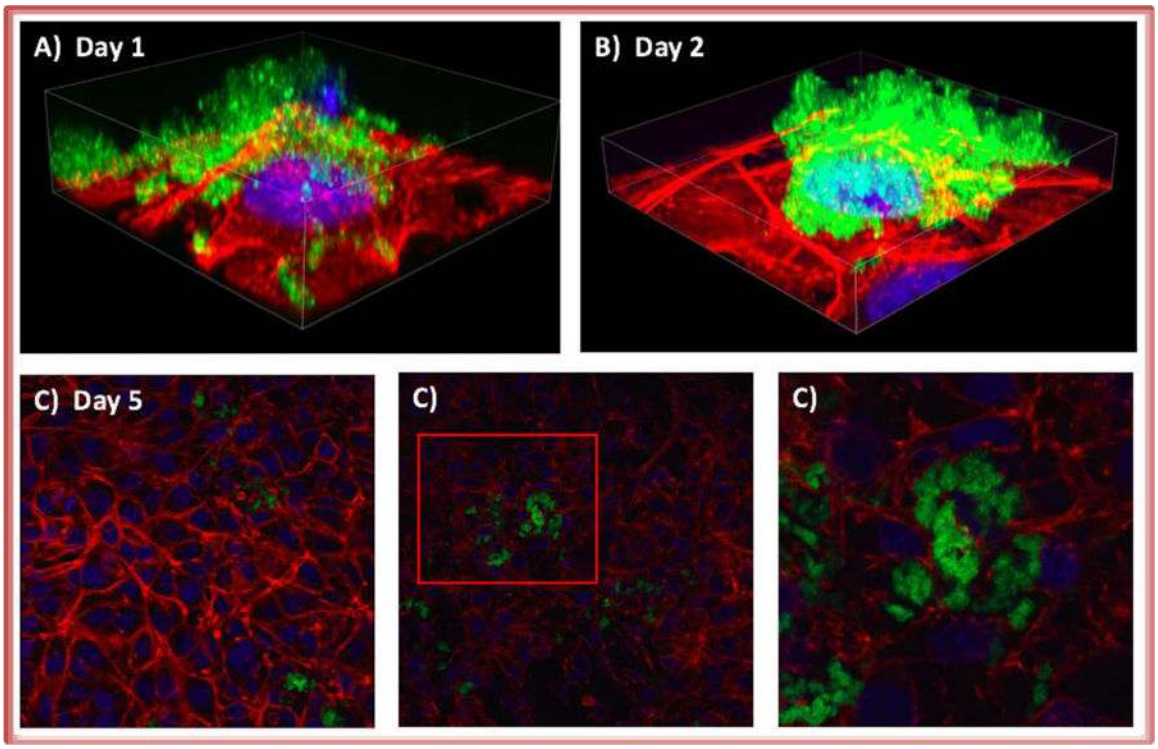

Figure 6.
Confocal microscopy results demonstrating cellular uptake after 5 Days in culture conditions using a 40μL JBNT dose.

Table 1

NP Sizes and Zeta Potentials with fluorescence siRNA. N=50.

JBNT Data (fluorescence siRNA adjusted to 2μL siRNA)				
siRNA (μL)	**JBNT (μL)**	**Nuclease Free Water (μL)**	**Size (nm)**	**Zeta Potential (mV)**
2	2	20	59	−23
2	15	20	702	−5
2	30	20	490	9
2	40	20	240	21

Table 2

NP Size and Zeta Potential with standard siRNA. N=50

JBNT Data (standard siRNA adjusted to 2μL siRNA)				
siRNA (μL)	**JBNT (μL)**	**Nuclease Free Water (μL)**	**Size (nm)**	**Zeta Potential (mV)**
2	2	20	79	−41
2	4	20	319	−26
2	10	20	589	−8
2	15	20	623	−1
2	20	20	579	5
2	30	20	222	12
2	40	20	169	20

Table 3

Tabulated organization of JBNT doses ranging from 2–40μL with corresponding lengths and widths (at a 2μL siRNA dose). N=50.

JBNT Average Length and Width by JBNT Dose				
JBNT Dose (μL)	**Average Length (nm)**	**Length Std. Dev. (nm)**	**Average Width (nm)**	**Width Std. Dev. (nm)**
2 JBNT	151	52	20	6
15 JBNT	183	57	23	8
30 JBNT	193	48	18	4
40 JBNT	270	65	20	4